A numerical approach to study the Kramers equation for finite geometries: boundary conditions and potential fields

Adérito Araújo[1], **Amal K Das**[2] **and Ercília Sousa**[1]

[1] CMUC, Department of Mathematics, University of Coimbra, 3001-501 Coimbra, Portugal
[2] Department of Physics, Dalhousie University, Halifax, Nova Scotia B3 H 3J5, Canada

E-mail: ecs@mat.uc.pt

Abstract

The Kramers equation for the phase-space function, which models the dynamics of an underdamped Brownian particle, is the subject of our study. Numerical solutions of this equation for natural boundaries (unconfined geometries) have been well reported in the literature. But not much has been done on the Kramers equation for finite (confining) geometries which require a set of additional constraints imposed on the phase-space function at physical boundaries. In this paper we present numerical solutions for the Kramers equation with a variety of potential fields—namely constant, linear, harmonic and periodic—in the presence of fully absorbing and fully reflecting boundary conditions (BCs). The choice of the numerical method and its implementation take into consideration the type of BCs, in order to avoid the use of ghost points or artificial conditions. We study and assess the conditions under which the numerical method converges. Various aspects of the solutions for the phase-space function are presented with figures and discussed in detail.

Keywords: Kramers equation, absorbing boundaries, reflecting boundaries, potential fields, numerical methods

1. Introduction

Overdamped Brownian motion, modeled by the Fickian diffusion equation and for finite geometries, has been extensively studied—both analytically and numerically [15]. The effect

of finite geometries is taken into account through various boundary conditions (BCs), with respect to one or more space variables, on the probability density function which is the solution of the diffusion equation for the problem at hand. The diffusion equation may describe a free Brownian particle (i.e. in the absence of a potential field) or may include a potential field. Quite recently we have discussed numerical solution of the non-Fickian diffusion equation. The reader is referred to [1] for details of this work.

In this work we shall consider underdamped Brownian motion which is modeled by the Kramers equation [35]. This is a phase-space Fokker–Planck equation and from which the usual Fickian diffusion equation and a somewhat unusual non-Fickian diffusion equation can both be derived [17].

An equivalent modelling of underdamped Brownian motion is done through the Langevin equation which includes the intertial term. We refer to [14] for a detailed account of the Langevin equation. In our work we shall focus on the Kramers equation. Underdamped Brownian dynamics described by the Kramers equation in the x-p space and not in x-space alone and in confined geometry have not been much studied.

The Kramers equation can describe short-time (inertial) as well as long-time (diffusive) motion of the Brownian particle. If we consider infinite geometries then it is assumed and physically anticipated that the probability density function will vanish at infinite distances from the source. But the situation can be different if we consider finite geometries. We shall deal with this situation in this paper.

Let us introduce the time-dependent Kramers equation for the single-particle distribution function in position and momentum variables, and in the presence of an external (time-independent but space-dependent) external potential field:

$$\frac{\partial f}{\partial \bar{t}} + \frac{\bar{p}}{m}\frac{\partial f}{\partial \bar{x}} + F(\bar{x})\frac{\partial f}{\partial \bar{p}} = \bar{\gamma}\frac{\partial}{\partial \bar{p}}\left(\bar{p}f\right) + mk_{\mathrm{B}}T\bar{\gamma}\frac{\partial^2 f}{\partial \bar{p}^2}, \tag{1}$$

where $\bar{x}$ is the position component, $\bar{p}$ is the momentum component of the Brownian particle, $\bar{t}$ is the time, $\bar{\gamma}$ is a friction parameter, $k_{\mathrm{B}} = 1.38 \times 10^{-16}\,\mathrm{erg} \times K^{-1}$ is the Boltzmann constant, $T = 300$ K is the room temperature, $m = 10 \times 10^{-10}$ gm is the mass of a Brownian particle and F is the force acting on the particle from the potential field V, that is

$$F(\bar{x}) = -\frac{\mathrm{d}V}{\mathrm{d}\bar{x}}(\bar{x}). \tag{2}$$

For a numerical study of the Kramers equation, it is more convenient to introduce the following scaled variables

$$x = \frac{\bar{x}}{k_{\mathrm{B}}T}; \quad t = \bar{t}\sqrt{mk_{\mathrm{B}}T}; \quad p = \frac{\bar{p}}{\sqrt{mk_{\mathrm{B}}T}}; \quad \gamma = \frac{\bar{\gamma}}{\sqrt{mk_{\mathrm{B}}T}}; \quad V(x) = \frac{1}{k_{\mathrm{B}}T}V(\bar{x}) \tag{3}$$

in order to obtain the Kramers equation in the form

$$\frac{\partial f}{\partial t} + p\frac{\partial f}{\partial x} + F\frac{\partial f}{\partial p} = \gamma\frac{\partial}{\partial p}(pf) + \gamma\frac{\partial^2 f}{\partial p^2}. \tag{4}$$

Analytic solutions of the Kramers equation (in phase-space) or even Fokker–Planck equations (in x- or p-space alone) can be found only in some special cases (see for instance [5, 35]). In general it is difficult to obtain exact analytical solutions of the Kramers equation. Because few exact analytical solutions are available specially for finite geometries, numerical methods have become a significant resource in the study of the behaviour of the solutions, playing an important role in new explorations of phase-space stochastic processes.

The difficulties of dealing with Kramers equation numerically come from several factors. Firstly, this problem behaves like a parabolic equation in the p-direction, and behaves like a hyperbolic equation in the x-direction. Secondly, we have different types of hyperbolic equations in the x-directions, for $p > 0$ and $p < 0$, respectively. Consequently, the solution may satisfy different kinds of BCs on different subdomains. Therefore, we have to use domain decomposition and different approximations on different subdomains. This leads to additional difficulties in actual computation and numerical analysis.

We briefly recall the theoretical and numerical approaches in the literature to solve the Fokker–Planck and the Kramers equations. Motivated by the work due to Brinkman [4] and also developed in [39], a class of analytical and numerical methods have been proposed, by utilizing a set of orthogonal functions in velocity (or momentum) variables as a spectral basis. The rationale behind this approach lies in the fact that the set of orthogonal functions, usually Hermite polynomials, form a complete system and satisfy correct natural BCs in momentum space. However, in the case of a phase-space equation like the Kramers equation, the subsequent approximate route through orthogonal polynomials has been used only for the open p-space but not for the bounded x-space. Once we impose BCs in x-space, this route is not easily applicable anymore.

The analytical methods motivated by [4] consists essentially of expanding the distribution function in an appropriate set of orthogonal functions. If the variable p (or x) extend from minus to plus infinity (natural BCs) we may use for instance Hermite functions and then $f(x, p, t)$ can be expanded in terms of these set of functions or in the case of periodic BCs a Fourier series can be used. By inserting this expansion in the Fokker–Planck equation or Kramers equation we obtain an infinite system of coupled differential equations for the coefficients. Reducing the infinite system to a finite system leads to approximate solutions. Then the finite system can be solved by a matrix continued fraction method. This methodology is developed in great detail in [35] and more recently in the context of the Langevin equation in [14], where its many advantages are explored; it is useful to derive analytical results, as can be seen for instance in [12, 13, 16, 24]. This approach can also be used to obtain the solutions of the Kramers equation numerically, although for the purpose of studying the numerical behaviour of the phase-space distribution it may not be the most direct method. It is worth noting that according [35], for certain potentials the dimensions of the matrices involved can become too large for an efficient computation. Therefore, alternative numerical methods have been appearing in literature.

Among the numerical methods motivated by the use of orthogonal polynomials, a common approach is based on the Hermite and Legendre approximations for the open space p, see, e.g., [20, 21, 40, 42]. For instance, in [20] the authors proposed a Hermite expansion in the phase space combined with finite differences in time and space. However, the finite difference approximation in the x-direction limits the higher numerical accuracy that can be reached in the p-direction. Additionally the Hermite expansion cannot produce a reasonable approximation or with high numerical accuracy without carefully choosing a scaling factor [43], which depends on the type of solutions we are approximating. In [20] the authors also observe that the high order accuracy is reached more easily for large times or when we approach a stationary solution. Stationary solutions for the Kramers equation can occur for instance in the cases we have a non-pathological potential field and reflective BCs in a finite geometry or for a periodic potential and natural BCs in an infinite geometry. However, many cases of interest are not necessarilly related with stationary solutions, such as, if we have absorbing boundaries and a potential field not abnormaly high or for mixed BCs (one absorbing and one reflecting) in the absence of a potential field.

Other type of numerical algorithms have been proposed for solving the Kramers equation, such as [8–11, 19, 31]. In [8, 9, 11], numerical solutions of the Kramers equation for a periodic potential and for natural boundaries i.e. for infinite geometries ($-\infty < x < \infty$) have been reported. In [19] a numerical solution, for semi-infinite geometry, $x > 0$, is presented for the time-Laplace transform of the backward Kramers equation from which the mean first-passage time can be obtained. In [10, 44] implicit finite difference schemes are used and in [31] Galerkin methods are considered which approach does not seem easily generalizable for certain BCs, namely mixed BCs.

In this paper we report on numerical solutions of the Kramers equation in finite geometries which entail BCs that are imposed on theoretical considerations and implemented numerically. In addition to considering finite geometries we include potential fields of various types in the Kramers equation. This leads to a numerical study of an interplay between BCs and potential fields.

The numerical method presented has the merit of being flexible and easily implemented to obtain numerical approximations for the phase space distribution function as we change the potential field and the BCs. It is an explicit method that efficiently deals with different types of potential fields. Also the BCs are implemented without any artifitial approximation or tecnhique. For instance, the way we implement the reflecting BCs is more natural and efficient than the way the reflecting BCs are implemented in [10]. Many times explicit methods are avoided because to take advantage of its full efficiency we need to know their stability regions, usually not easy to find, although quite relevant. Therefore, we present a theorem on the stability of the numerical method, which allows us to choose the step sizes in time, space and phase space adequately, that is, in order to remain inside the convergence region of the numerical method.

Two types of BCs are studied in this paper: absorbing and reflecting BCs. The BCs and physical considerations associated with them are presented in section 2. And in that section we refer to some previous works (analytical and numerical) which consider a semi-infinite geometry and absorbing BCs. The numerical method we have used for the problem at hand and its convergence are discussed in detail in section 3. Numerical results for the phase-space function $f(x, p, t)$ for several potential fields and other quantities of interest are presented and discussed in section 4. Section 5 contains some general discussion and outlook.

2. BCs: physical considerations

We consider the Kramers equation for the domain

$$\Omega = \left\{ (x, p): x_{\mathrm{L}} < x < x_{\mathrm{R}}; \quad -\infty < p < \infty \right\}. \tag{5}$$

This means that we consider a finite domain in space but all values of momenta are included. We assume an initial condition of the form

$$f(x, p, 0) = f_0(x, p), \quad (x, p) \in \Omega. \tag{6}$$

This initial condition is specified by two narrow Gaussians, located in the middle of the domain

$$f(x, p, 0) = g_1(x) g_2(p), \quad (x, p) \in \Omega, \tag{7}$$

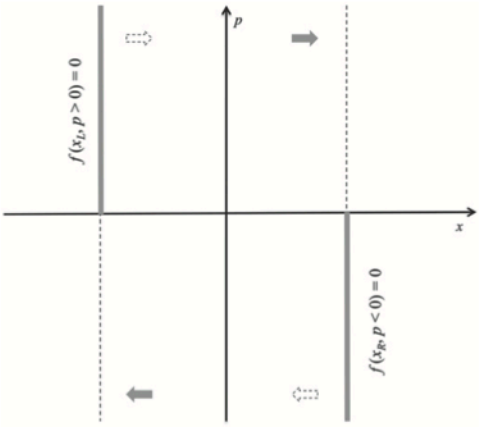

Figure 1. Absorbing boundary conditions. The heavy arrows show a non-zero flux S_x defined by (11) at the left and right boundaries; the light arrows illustrate the conditions $S_x(x_L, p > 0, t) = 0$ and $S_x(x_R, p < 0, t) = 0$.

where

$$g_1(x) = \frac{1}{\epsilon\sqrt{\pi}} e^{-(x-c)^2/\epsilon^2}, \quad g_2(p) = \frac{1}{\epsilon\sqrt{\pi}} e^{-p^2/\epsilon^2}, \tag{8}$$

for $c = (x_R + x_L)/2$ and small values of ϵ.

Although we consider a variety of potentials $V(x)$ and hence $F(x)$, the initial condition is assumed to be the same for all these cases. And for all these cases, when p goes to $\pm\infty$ we assume that

$$\lim_{p\to-\infty} f(x, p, t) = 0, \quad \lim_{p\to\infty} f(x, p, t) = 0, \qquad x_L < x < x_R, \quad t > 0, \tag{9}$$

i.e., there is negligible probability of finding the Brownian particle with infinite momenta/ velocities (positive or negative).

We now come to one of the central themes of our work, the spatial BCs at $x = x_L$ and at $x = x_R$. These are absorbing and reflecting BCs first proposed by Wang and Uhlenbeck [41].

2.1. Absorbing BCs

The absorbing BCs are also considered in more recent works, such as, Bicout *et al* [2], and by Singer and Schuss [36]. The absorbing BCs at $x = x_L$ and $x = x_R$, illustrated in figure 1, are given by

$$f(x_L, p, t) = 0, \quad p > 0, \quad t > 0, \qquad f(x_R, p, t) = 0, \quad p < 0, \quad t > 0. \tag{10}$$

As can be seen from (10), these BCs each affect one half range of p's.

In order to understand these BCs physically, let us assume that the Brownian particle is in the domain whose interior is bounded by x_L (on the left) and by the boundary at x_R (on the right). The momentum of the particle and hence the velocity $v(= p/m)$ are assumed to be positive from the boundary at x_L into the interior, and negative from the boundary at x_R into the interior. Since the boundary at x_L is absorbing, there is no particle flux from the boundary at x_L into the interior for positive momentum.

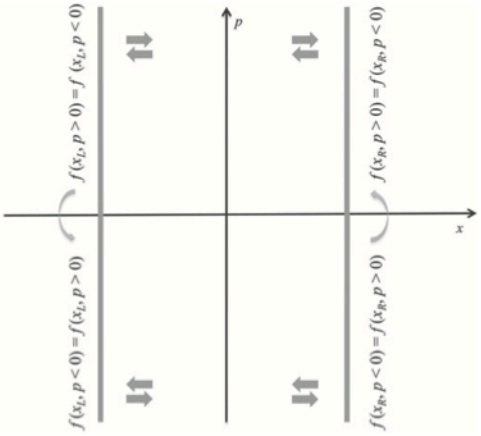

Figure 2. Reflecting boundary conditions. The heavy arrows state a non-zero flux S_x defined by (11) and also illustrates the condition $S_x(x_{\mathrm{L}}, p, t) = -S_x(x_{\mathrm{R}}, p, t)$.

The absorbing BCs can be illustrated through a consideration of particle flux S_x defined as (see Risken [35], page 183)

$$S_x(x, p, t) = (p/m)f(x, p, t). \tag{11}$$

The flux from the interior toward the left boundary is non-zero (for $p < 0$), while the flux S_x (for $p > 0$) from the left boundary toward the interior is vanishing. These fluxes are shown in figure 1, as a heavy arrow and as a light arrow respectively. The reverse situation occurs for the right boundary as also illustrated in figure 1. Since the flux S_x defined in (11) vanishes at x_{L} for $p > 0$, then $f(x, p, t)$ at x_{L} vanishes for $p > 0$ which is the first BC in (10). An opposite situation occurs at the boundary at x_{R} , which leads to the second BC in (10).

This feature makes these BCs interesting in both analytical and numerical studies of underdamped Brownian motion modeled by the Kramers equation. Discussions about the existence of solution of the Kramers equation for absorbing BCs can be found, for example, in [6, 7, 27]. In [27] the authors state that for a linear potential and for semi-infinite geometry $[0, \infty)$ the Kramers equation can be argued to possess a unique solution (with a delta-function initial condition). There is some previous work [19] in which first passage times were studied through a combination of power series expansion applied to the time-Laplace transformed Kramers equation together with a numerical approximation of second-order difference. But in that work, a full time-Laplace inversion was not reported.

In our work we discretize the time-dependent Kramers equation for finite geometries, directly in time, space and momentum variables. We consider boundaries (i) both absorbing, (ii) both reflecting, (iii) one reflecting and the other absorbing boundaries. Also we consider a variety of potential fields—the other central theme of our work.

2.2. Reflecting BCs

We turn now to the reflecting BCs. They read

$$f(x_{\mathrm{L}}, p, t) = f(x_{\mathrm{L}}, -p, t) \qquad f(x_{\mathrm{R}}, p, t) = f(x_{\mathrm{R}}, -p, t). \tag{12}$$

These conditions are illustrated in figure 2. These BCs indicate that the phase-space distribution function $f(x, p, t)$ is assumed to be symmetric in p at $x = x_{\mathrm{L}}$ and $x = x_{\mathrm{R}}$. But

$f(x_L, p, t)$ and $f(x_R, p, t)$ themselves are otherwise unspecified or undetermined. On physical grounds, the reflecting BCs mean that no particle would be lost at the boundary and all particles with p and $-p$ will be reflected back into the interior.

In terms of the flux, introduced in section 2.1, defined by (11), for the reflecting BCs the two fluxes going from the interior toward the boundaries and those from the boundaries going toward the interior are both non-zero. These are shown as thick arrows in figure 2.

3. Numerical method and convergence

In this section we describe the numerical method used to derive approximate solutions for the Kramers equation, giving special attention to how we incorporate the BCs. The numerical method is an explicit method and therefore is conditionally stable. We provide details on the convergence of the numerical method, which include the derivation of the stability conditions. Although explicit methods are conditionally stable, as long as the stability conditions are not very strict, they have the advantage of being computationally more efficient than implicit numerical methods.

3.1. Numerical method

We can rewrite the differential equation (4) in the form

$$\frac{\partial f}{\partial t} + p\frac{\partial f}{\partial x} + (F - \gamma p)\frac{\partial f}{\partial p} = \gamma f + \gamma \frac{\partial^2 f}{\partial p^2}. \tag{13}$$

We consider the computational domain

$$\overline{\Omega} = \left\{ (x, p): x_L \leqslant x \leqslant x_R, \quad p_L \leqslant p \leqslant p_R \right\} \tag{14}$$

and the uniform grid in $\overline{\Omega}$ defined by

$$\left\{ (x_j, p_k): x_j = x_L + (j-1)\Delta x, \quad p_k = p_L + (k-1)\Delta p \right\}, \tag{15}$$

where

$$\Delta x = \frac{x_R - x_L}{N_x}, \qquad \Delta p = \frac{p_R - p_L}{N_p}. \tag{16}$$

The discretization in time is defined in the interval $[0, T]$ at the points

$$t_n = (n-1)\Delta t, \qquad \Delta t = \frac{T}{N_t}. \tag{17}$$

The approximate solution, defined in the discrete domain given by (15)–(17), which approximates $f(x_j, p_k, t_n)$, is denoted by $f^n_{j,k}$. Before presenting the numerical method, we define the following discretization operators

$$\Delta_p f^n_{j,k} = \frac{1}{2}\left(f^n_{j,k+1} - f^n_{j,k-1}\right), \qquad \delta^2_p f^n_{j,k} = f^n_{j,k+1} - 2f^n_{j,k} + f^n_{j,k-1} \tag{18}$$

and also

$$\delta^+_x f^n_{j,k} = f^n_{j+1,k} - f^n_{j,k}, \qquad \delta^-_x f^n_{j,k} = f^n_{j,k} - f^n_{j-1,k}. \tag{19}$$

The numerical method considered to approximate (13) is given by

$$f_{j,k}^{n+1} - f_{j,k}^{n} + \frac{p_k \Delta t}{\Delta x}\delta_x f_{j,k}^{n} + \left(F_j - \gamma p_k\right)\frac{\Delta t}{\Delta p}\Delta_p f_{j,k}^{n} = \gamma \Delta t f_{j,k}^{n} + \frac{\gamma \Delta t}{\Delta p^2}\delta_p^2 f_{j,k}^{n}, \tag{20}$$

where $F_j = F(x_j)$ and the operator $\delta_x f_{j,k}^{n}$ is defined by taking into account the x-direction of the flow, that is

$$\delta_x f_{j,k}^{n} = \begin{cases} \delta_x^{-} f_{j,k}^{n} & \text{if } p_k > 0, \\ \delta_x^{+} f_{j,k}^{n} & \text{if } p_k < 0. \end{cases} \tag{21}$$

In order to compute the solution, we rewrite the previous system in a matrix form and our goal is to determine a vector, in the instant t_{n+1}, of the form

$$\mathbf{F}^{n+1} = \Big[f_{1,1}^{n+1}, f_{2,1}^{n+1}, \ldots, f_{N_x+1,1}^{n+1}, f_{1,2}^{n+1}, f_{2,2}^{n+1}, \ldots, f_{N_x+1,2}^{n+1}, \ldots, f_{1,N_p+1}^{n+1}, f_{2,N_p+1}^{n+1}, \ldots, f_{N_x+1,N_p+1}^{n+1}\Big]^T, \tag{22}$$

that is

$$\mathbf{F}^{n+1} = M\mathbf{F}^{n}, \tag{23}$$

where M is the matrix iteration. To build the matrix M we need to take into account the BCs. The vector $\mathbf{F}^n$ is built by organizing the grid points columnwise from the upper left to the lower right and it has $(N_x - 1) \times (N_p - 1)$ interior points.

3.2. Implementation of BCs

In this section, we give an overview of how to implement the boundary conditions. In the direction p, the physical problem does not have boundaries; therefore, since the computational domain needs to be bounded, we consider the computational domain large enough, so we can assume the numerical BC

$$f\left(x_j, p_{\mathrm{L}}, t_n\right) = f\left(x_j, p_{\mathrm{R}}, t_n\right) = 0, \quad \text{for all} \quad x_j, t_n. \tag{24}$$

Additionally, we consider $p_{\mathrm{R}} = -p_{\mathrm{L}} = \mathrm{L}$ for L large enough, that is, L is such that the condition $f(x, p, t) = 0$, for $|p| > \mathrm{L}$, is a physical condition. In this way the numerical boundary conditions do not interfere with the accuracy of the numerical solution.

In the x direction we consider two types of BCs: absorbing and reflecting. We start to describe the implementation of the absorbing BCs. In this case we only have physical boundaries defined at $x = x_{\mathrm{L}}$ for $p > 0$ and at $x = x_{\mathrm{R}}$ for $p < 0$, that is

$$f\left(x_{\mathrm{L}}, p_k, t_n\right) = 0, \text{ for } \quad p_k > 0 \tag{25}$$

$$f\left(x_{\mathrm{R}}, p_k, t_n\right) = 0, \text{ for } \quad p_k < 0. \tag{26}$$

The first derivative in the space variable x is approximated by the discretization operator δ_x defined in (21) taking into consideration the type of boundaries we are assuming, in order to avoid the use of ghost points or artificial conditions. When $p_k > 0$, to compute the approximation value of the derivative at (x_j, p_k, t_n) we use the values $f_{j,k}^{n}$ and $f_{j-1,k}^{n}$ and therefore we can compute the approximation value at the boundary point $x = x_{\mathrm{R}}$, denoted by $f_{N_x+1,k}^{n}$, by an interpolation of the values $f_{N_x+1,k}^{n}$ and $f_{N_x,k}^{n}$.

Similarly, for $p_k < 0$, the discretization of the derivative at (x_j, p_k, t_n) uses the approximation values $f^n_{j,k}$ and $f^n_{j+1,k}$ and therefore to compute the boundary value at $x = x_L$, denoted by $f^n_{1,k}$, we interpolate the values $f^n_{1,k}$ and $f^n_{2,k}$.

For the case of reflecting BCs, we have the conditions

$$f\left(x_L, p_k, t_n\right) = f\left(x_L, -p_k, t_n\right), \tag{27}$$

$$f\left(x_R, p_k, t_n\right) = f\left(x_R, -p_k, t_n\right). \tag{28}$$

As we have described for the absorbing BCs for $p_k > 0$, we only need to access boundary values at $x = x_L$ and similarly for $p_k < 0$ we only need the boundary values at $x = x_R$. Therefore we proceed in the following way. For $p_k > 0$, to compute the nearest point to the boundary $x = x_L$, which is denoted by $f^n_{2,k}$ we need to interpolate the values $f^n_{1,k}$ and $f^n_{2,k}$, where $f^n_{1,k}$ denotes the approximation value of $f(x_L, p_k, t_n)$. To impose the reflecting BC (27) we use the approximation point of $f(x_L, -p_k, t_n)$ instead of the approximation point $f^n_{1,k}$ of $f(x_L, p_k, t_n)$. For $p_k < 0$ we proceed similarly, near the right boundary $x = x_R$.

To have a better understanding about the implementation we describe below the matricial structure.

Concerning the boundary points related to $p = p_L$ they are $[f^n_{1,1}, f^n_{2,1}, ..., f^n_{N_x+1,1}]^T$ which, on the vector (22), corresponds to the entries $\mathbf{F}^n_r$, $r = 1, ..., N_x + 1$ and the boundary points related to $p = p_R$ are $[f^n_{1,N_p+1}, f^n_{2,N_p+1}, ..., f^n_{N_x+1,N_p+1}]^T$ which, on the vector (22), corresponds to the entries $\mathbf{F}^n_{N_p^*(N_x+1)+r}$, $r = 1, \ldots, N_x + 1$.

Similarly, the boundary points related to $x = x_L$ are $[f^n_{1,1}, f^n_{1,2}, ..., f^n_{1,N_p+1}]^T$ which, on the vector (22), corresponds to the entries $\mathbf{F}^n_{r(N_x+1)-N_x}$, $r = 1, \ldots, N_p + 1$ and the boundary points related to $x = x_R$ are $[f^n_{N_x+1,1}, f^n_{N_x+1,2}, ..., f^n_{N_x+1,N_p+1}]^T$ which, on the vector (22), corresponds to the entries $\mathbf{F}^n_{r(N_x+1)}$, $r = 1, \ldots, N_p + 1$.

Therefore, the BCs for the absorbing boundary case are implemented by imposing

$$\mathbf{F}^n_r = \mathbf{F}^n_{N_p(N_x+1)+r} = 0, \qquad r = 1, \ldots, N_x + 1, \tag{29}$$

$$\mathbf{F}^n_{r(N_x+1)-N_x} = 0, \qquad r = 2, \ldots, \frac{N_p}{2}, \tag{30}$$

$$\mathbf{F}^n_{r(N_x+1)} = 0 \qquad r = \frac{N_p}{2} + 2, \ldots, N_p. \tag{31}$$

For the reflecting BCs we have

$$\mathbf{F}^n_r = \mathbf{F}^n_{N_p(N_x+1)+r} = 0, \qquad r = 1, \ldots, N_x + 1, \tag{32}$$

$$\mathbf{F}^n_{r(N_x+1)-N_x} = \mathbf{F}^n_{(Np+2-r)(Nx+1)-Nx}, \qquad r = 2, \ldots, \frac{N_p}{2}, \tag{33}$$

$$\mathbf{F}^n_{r(Nx+1)} = \mathbf{F}^n_{(Np+2-r)(Nx+1)}, \qquad r = \frac{N_p}{2} + 2, \ldots, N_p. \tag{34}$$

For physical problems at hand, whose results will be presented in section 4, we have also considered $x_L = -x_R$. And in order to include discrete points corresponding to $p = 0$, we need to assume N_p to be even.

3.3. Convergence of the method

From the way we have derived the numerical method it is straightforward to obtain the truncation error of the numerical method to conclude that the numerical method has first order accuracy regarding the time variable and the space variable and second order accuracy regarding the momentum variable, that is, $O(\Delta x + \Delta p^2 + \Delta t)$.

Next we are interested in analyzing the stability of the numerical method for the Kramers equation, which has variable coefficients. Results for linear equations with variable coefficients were initially given by Lax [25, 26] for a hyperbolic one dimensional problem. Generalizations to parabolic equations, multidimensional problems and systems of equations can be found in [32, 34, 37]. To analyze the stability of our method we can apply the following result, that can be found in [34, 37].

Consider the finite difference method for equation (4), of the form

$$f_{j,k}^{n+1} = Q f_{j,k}^{n}, \tag{35}$$

with

$$Q = \sum_{l=-l_1}^{l_2} \sum_{m=-m_1}^{m_2} c_{l,m}(x, p) S^{l+m},$$

where the coefficients $c_{l,m}(x, p)$ are functions of x and p and S^{l+m} represents the forward and backward shift operators, that is

$$S^{l+m} f_{j,k}^{n} = f_{j-l,k-m}^{n}.$$

A consistent method is stable if the function

$$\rho(x, p, \xi) = \sum_{l=-l_1}^{l_2} \sum_{m=-m_1}^{m_2} c_{l,m}(x, p) \mathrm{e}^{-\mathrm{i}l\xi_x} \mathrm{e}^{-\mathrm{i}l\xi_p}, \quad \xi = \left(\xi_x, \xi_p\right), \tag{36}$$

satisfies

(a) it is Lipschitz continuous in (x, p);
(b) for $\xi \neq 0$ and $\max\{|\xi_x|, |\xi_p|\} \leqslant \pi$, we have

$$|\rho(x, p, \xi)| < 1 + O(\Delta t) \qquad \text{for all } (x, p);$$

(c) for $\max\{|\xi_x|, |\xi_p|\} \leqslant \pi$, Δt less than some $\tau > 0$ and $\delta(x, p) > 0$, for all (x,p),we have

$$|\rho(x, p, \xi)| \leqslant 1 + O(\Delta t) - \delta(x, p)|\xi|^{2q},$$

where $q > 0$ and $|\xi|^2 = \xi_x^2 + \xi_p^2$.

The following result concerns the stability of the method (20) and the proof follows some ideas presented in [23, 37]. The von Neumann method can be applied to Cauchy problems or bounded domains assuming the boundaries are periodic. Nevertheless, for many types of boundaries the stability conditions obtained through the von Neumann analysis are very close to the necessary and sufficient condition for practical stability [22, 38].

Theorem 1. *Let*

$$C_1 = \|p\|_\infty \, \nu_x + 2\mu \qquad \text{and} \qquad C_2 = \|p\|_\infty \, \nu_x + \|F - \gamma p\|_\infty^2 \, \frac{\nu_p^2}{2\mu}, \tag{37}$$

where $\|p\|_\infty = \max_k\{|p_k|\}$, $\|F - \gamma p\|_\infty = \max_{j,k}|F_j - \gamma p_k|$ *and*

$$\nu_x = \frac{\Delta t}{\Delta x}, \qquad \nu_p = \frac{\Delta t}{\Delta p}, \qquad \mu = \gamma \frac{\Delta t}{\Delta p^2}. \tag{38}$$

If

$$C_1 \leqslant 1 \qquad \text{and} \qquad C_2 \leqslant 1, \tag{39}$$

then the amplification factor for the numerical method (20) satisfies the conditions (a)–(c) stated previously.

Proof. (a) We assume the function F, defined by (2), is smooth and therefore the Lipschitz continuous condition is trivially satisfied. (b) Now, we will derive the amplification factor, when $p \geqslant 0$. If $p < 0$, the operator δ_x is given by the upwind approximation and the expression of the amplification factor changes slightly. However, it is easy to see that the result follows in a similar way.

For the numerical method (20), the amplification factor for $p_k \geqslant 0$ is given by

$$\begin{aligned}\rho\big(x_j, p_k, \xi\big) = (1 + \gamma\Delta t) - p_k\nu_x\big(1 - \mathrm{e}^{-\mathrm{i}\xi_x}\big) \\ - \frac{1}{2}\big(F_j - \gamma p_k\big)\nu_p\big(\mathrm{e}^{\mathrm{i}\xi_p} - \mathrm{e}^{-\mathrm{i}\xi_p}\big) + \mu\big(\mathrm{e}^{\mathrm{i}\xi_p} - 2 + \mathrm{e}^{-\mathrm{i}\xi_p}\big),\end{aligned} \tag{40}$$

where $\xi = (\xi_x, \xi_p)$.

For clarity, we denote

$$\nu_k = p_k\nu_x \qquad \text{and} \qquad \beta_{j,k} = \big(F_j - \gamma p_k\big)\nu_p.$$

We can write

$$\rho\big(x_j, p_k, \xi\big) = (1 + \gamma\Delta t) - \nu_k\big(1 - \cos\xi_x\big) - 2\mu\big(1 - \cos\xi_p\big) + i\nu_k \sin\xi_x + i\beta_{j,k}\sin\xi_p,$$

and therefore

$$|\rho|^2 = \Big[(1 + \gamma\Delta t) - \nu_k\big(1 - \cos\xi_x\big) - 2\mu\big(1 - \cos\xi_p\big)\Big]^2 + \Big[\nu_k \sin\xi_x + \beta_{j,k}\sin\xi_p\Big]^2.$$

Applying the Cauchy–Schwartz inequality we obtain

$$\begin{aligned}\Big(\nu_k\sin\xi_x + \beta_{j,k}\sin\xi_p\Big)^2 &= \left(\frac{\nu_k}{\sqrt{\nu_k}}\sqrt{\nu_k}\,\sin\xi_x + \frac{\beta_{j,k}}{\sqrt{2\mu}}\sqrt{2\mu}\,\sin\xi_p\right)^2 \\ &\leqslant \left(\frac{\nu_k^2}{\nu_k} + \frac{\beta_{j,k}^2}{2\mu}\right)\Big(\nu_k\sin^2\xi_x + 2\mu\sin^2\xi_p\Big) \\ &\leqslant \nu_k\sin^2\xi_x + 2\mu\sin^2\xi_p,\end{aligned}$$

since, from (39), $\nu_k + \beta_{j,k}^2/2\mu \leqslant 1$. Let $s_x = 1 - \cos\xi_x$ and $s_p = 1 - \cos\xi_p$, we can write

$$\begin{aligned}
|\rho|^2 &\leqslant \Big[(1+\gamma\Delta t) - \nu_k s_x - 2\mu s_p\Big]^2 + \nu_k s_x\big(2 - s_x\big) + 2\mu s_p\Big(2 - s_p\Big) \\
&= (1+\gamma\Delta t)^2 - 2(1+\gamma\Delta t)\Big(\nu_k s_x + 2\mu s_p\Big) + \Big(\nu_k s_x + 2\mu s_p\Big)^2 \\
&\quad + \nu_k s_x\big(2 - s_x\big) + 2\mu s_p\Big(2 - s_p\Big) \\
&= (1+\gamma\Delta t)^2 - 2\gamma\Delta t\Big(\nu_k s_x + 2\mu s_p\Big) + \Big(\nu_k s_x + 2\mu s_p\Big)^2 - \nu_k s_x^2 - 2\mu s_p^2.
\end{aligned}$$

Using again Cauchy–Schwartz

$$\begin{aligned}
\Big(\nu_k s_x + 2\mu s_p\Big)^2 &\leqslant \big(\nu_k + 2\mu\big)\Big(\nu_k s_x^2 + 2\mu s_p^2\Big) \\
&\leqslant \nu_k s_x^2 + 2\mu s_p^2,
\end{aligned}$$

since, from (39), $\nu_k + 2\mu \leqslant 1$. Therefore

$$|\rho|^2 \leqslant (1+\gamma\Delta t)^2 - 2\gamma\Delta t\Big(\nu_k s_x + 2\mu s_p\Big).$$

We can then conclude that for $\xi_x \neq 0$ and $\xi_p \neq 0$

$$|\rho|^2 < (1+\gamma\Delta t)^2.$$

Then

$$|\rho| < 1 + \gamma\Delta t.$$

(c) We have $|\rho| = 1 + \gamma\Delta t$ at $\xi = 0$ and for the other values of ξ, by (b) we can conclude that the value decreases having its minimum for some $\xi > 0$ and less than π. For small values of ξ, we replace sin and cos by the first terms of the Taylor expansion about $\xi = 0$. We obtain

$$\begin{aligned}
|\rho|^2 &= \left[1 + \gamma\Delta t - \nu_k\frac{\xi_x^2}{2} - 2\mu\frac{\xi_p^2}{2}\right]^2 + \Big[\nu_k\xi_x + \beta_{j,k}\xi_p\Big]^2 \\
&= (1+\gamma\Delta t)^2 - 2(1+\gamma\Delta t)\left(\nu_k\frac{\xi_x^2}{2} + 2\mu\frac{\xi_p^2}{2}\right) + \Big(\nu_k\xi_x + \beta_{j,k}\xi_p\Big)^2,
\end{aligned}$$

for small values of $\xi = (\xi_x, \xi_p)$ and therefore we ignore the the values of $|\xi|^p$ for $p \geqslant 4$. We also have that

$$\begin{aligned}
|\rho|^2 &\leqslant (1+\gamma\Delta t)^2 - 2\left(\nu_k\frac{\xi_x^2}{2} + 2\mu\frac{\xi_p^2}{2}\right) + \Big(\nu_k\xi_x + \beta_{j,k}\xi_p\Big)^2 \\
&= (1+\gamma\Delta t)^2 - \boldsymbol{\xi}^T M\boldsymbol{\xi},
\end{aligned}$$

where

$$\boldsymbol{\xi} = \begin{bmatrix}\xi_x & \xi_p\end{bmatrix}^T \qquad M = \begin{bmatrix}\nu_k & 0 \\ 0 & 2\mu\end{bmatrix} - \begin{bmatrix}\nu_k^2 & \nu_k\beta_{j,k} \\ \nu_k\beta_{j,k} & \beta_{j,k}^2\end{bmatrix}.$$

It is easy to check that the eigenvalues of the matrix M are both positive under the assumption of conditions (39) and therefore the matrix is symmetric positive definite and $\boldsymbol{\xi}^T M\boldsymbol{\xi} > 0$. We have

$$|\rho| \leqslant \sqrt{(1+\gamma\Delta t)^2 - \boldsymbol{\xi}^T M \boldsymbol{\xi}}$$
$$= (1+\gamma\Delta t)\sqrt{1 - \frac{\boldsymbol{\xi}^T M \boldsymbol{\xi}}{(1+\gamma\Delta t)^2}}.$$

Now we replace $\sqrt{1-z}$ by the first terms of the Taylor expansion about $z = 0$. We obtain

$$|\rho| \leqslant 1 + \gamma\Delta t - \frac{\boldsymbol{\xi}^T M \boldsymbol{\xi}}{(1+\gamma\Delta t)}.$$

Since $\Delta t \leqslant \tau$, then

$$|\rho| \leqslant 1 + \gamma\Delta t - \frac{\boldsymbol{\xi}^T M \boldsymbol{\xi}}{(1+\gamma\tau)}.$$

By the Rayleigh–Ritz theorem, for real symmetric matrices

$$\boldsymbol{\xi}^T M \boldsymbol{\xi} \geqslant \lambda_{\min} |\xi|^2,$$

where $\lambda_{\min}$ is the smallest eigenvalue of M. It follows that

$$|\rho| \leqslant 1 + \gamma\Delta t - \delta|\xi|^2,$$

where $\delta = \lambda_{\min}/(1+\gamma\tau)$. □

From condition (24), we can infer f is periodic in p. In the x direction we are considering two types of boundaries: absorbing and reflecting.

For the absorbing boundaries, although they are not periodic, the resulting iterative matrices can be formulated as circulant matrices and therefore they have the same structure as when we assume periodic BCs [18, 38].

Regarding the reflecting boundaries, we can check numerically that the conditions obtained define sharp stability regions. For instance, in table 1, we present the case when $F = 2$, where we describe the behaviour of the numerical method, when we consider discretization steps that lead to different values of C_1 and C_2. When the conditions in (37) are violated, the method blows up, that is, it does not converge. A similar result is obtained, if we consider other type of functions F.

3.4. Test problem

In this section we consider a problem to test the accuracy of the numerical method. We use the test problem presented in [42]. The numerical method presented in section 3.1 is used to solve equation (13), defined in the space domain $x \in [-1, 1]$ with $F(x) = x$, $\gamma = 1$ and a non-homogeneous source term $s(x, p, t)$ on the right hand side. We assume absorbing BCs, whose implementation is described in section 3.2. The addition of the source term do not interfer with the implementation of the numerical method and therefore its efficiency can be equally tested for homogeneous or non-homogeneous equations. The main reason for choosing this test example is that its analytic solution can be found exactly. The test solution as reported in [42] for absorbing boundaries, is

$$f(x, p, t) = 2^{1/2}(t+2)^{-1/2}\left(1 - x^2 \mathrm{e}^{-\frac{1}{10}(t+1)\left(x|p|+p^2\right)}\right)\mathrm{e}^{-p^2/2}. \tag{41}$$

Table 1. Behaviour of the numerical method (20) in the presence of reflecting boundary conditions when different discretization steps are considered in order to obtain different values for the stability conditions (37).

C_1	C_2	State of convergence
1.5656	1.2800	Diverges
1.2809	1.0473	Diverges
0.9394	0.7680	Converges

Table 2. Errors defined by (42) for $t_n = 1$, $\Delta x = \Delta p$ and small step size in the t direction $\Delta t = 1.7e-04$.

Δx	Error	Rate
2/17	$6.452e-02$	
2/33	$4.229e-02$	0.64
2/65	$2.456e-02$	0.80
2/129	$1.321e-02$	0.90
2/257	$6.851e-03$	0.95

Table 3. Errors defined by (42) for $t_n = 1$ as Δp changes, for small space step $\Delta x = 2/2050$ and small time step $\Delta t = 4.4e-05$.

Δp	Error	Rate
10/17	$6.862e-02$	
10/33	$1.671e-02$	2.13
10/65	$4.045e-03$	2.09
10/129	$8.912e-04$	2.21
10/257	$1.450e-04$	2.63

The numerical errors are measured by the discrete norm

$$E(t_n) = \left(\Delta x \Delta p \sum_{j=1}^{N_x} \sum_{k=1}^{N_p} \left(f\left(x_j, p_k, t_n\right) - f_{j,k}^n \right)^2 \right)^{1/2}, \tag{42}$$

where $f(x_j, p_k, t_n)$ represents the exact solution at the point (x_j, p_k, t_n) and $f_{j,k}^n$ the respective numerical solution.

In table 2 we plot the the convergence rate errors for $\Delta x = \Delta p$. The step sizes in the t direction are chosen to be small in order to analyse the order of convergence in the x direction. In table 3 we plot the erros and the convergence rate for the approximation in the p direction. The step sizes both in t and x directions are chosen to be very small in order to observe the second order convergence rate in the p direction. These numerical results are in agreement with the theoretical analysis of the preceding sub-sections.

Finally in figures 3(a) and (b) we plot the exact solution $f(x, p, t)$ and the numerical solution respectively, showing that the numerical solution fits the exact solution very well.

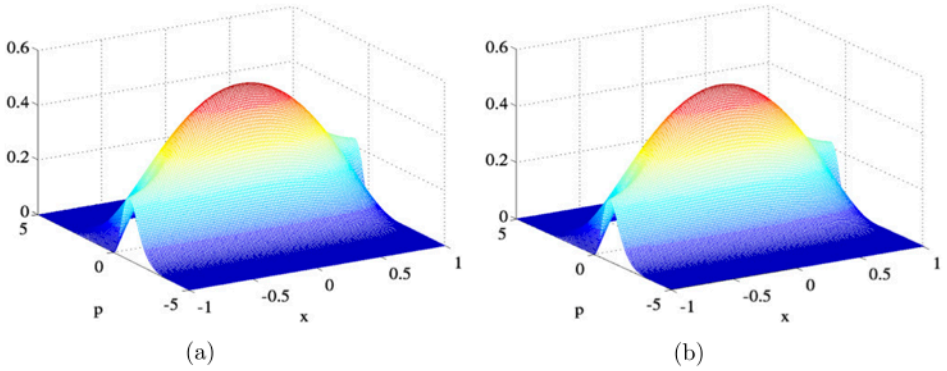

Figure 3. (a) Surface of the exact solution with absorbing boundary conditions; (b) surface of the numerical solution with absorbing boundary conditions. Solution at $t = 5$.

4. Numerical solutions

Using the numerical method presented in section 3, we have obtained solutions of the Kramers equation in the presence of absorbing and reflecting BCs, and with the initial condition specified in (7) and (8). Let us recall that our initial distribution is symmetrically located around $(x, p) = (0, 0)$. With the scaled variables introduced in (3), the Kramers equation as given by (4) has one input parameter γ and an input function $F(x) = -\mathrm{d}V(x)/\mathrm{d}x$. To obtain the numerical solutions we assume $\gamma = 1$ and the spatial domain is taken to be $-5 \leqslant x \leqslant 5$.

In this section we present some representative results from a detailed numerical study of solutions of the Kramers equation subject to absorbing and reflecting BCs (for finite geometries) and also in the presence of a variety of potential fields. The latter can affect the dynamics of the Brownian particle in addition to the BCs. We present results that show an interplay between BCs and potential fields. On general terms, the types of potential fields we consider are constant, attractive (confining), repulsive (de-confining) and periodic. Specific forms of potential fields are dealt with in the next sub-sections. For each type of potential we present figures for one particular instant of time. For each case we have selected the instant of time which we have found to be more illustrative of the effects of boundaries: absorbing and reflecting. It will be noted that the same instant of time is chosen for the same potential, first with absorbing BCs and then with reflecting BCs.

4.1. Absorbing BCs

We note that for the spatial domain we have chosen, the absorbing BCs are given by

$$f(-5, p, t) = 0, \quad \text{for } p > 0 \quad \text{and} \quad f(5, p, t) = 0 \quad \text{for } p < 0. \tag{43}$$

This equation indicates that $f(-5, p, t)$ for $p < 0$ and $f(5, p, t)$ for $p > 0$ are not affected by absorbing BCs. Interestingly, our computational results for $f(x, p, t)$ in the presence of certain potentials suggest that there is a symmetry relation between these two quantities. This is an empirical relation and is expressed as

$$f(-5, p < 0, t) = f(5, p > 0, t) \qquad \text{for all } t. \tag{44}$$

We shall invoke this relation to study an interplay between absorbing BCs and the type of potential fields. To explore this interplay we consider six potentials some of which lead to (44).

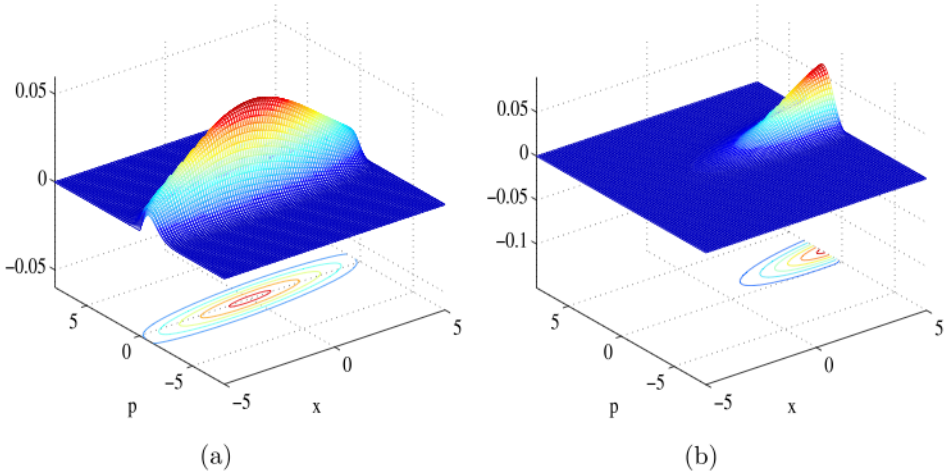

Figure 4. Surfaces and contour lines of the numerical solution $f(x, p, t)$ with absorbing boundary conditions (43); (a) homogeneous potential field $V(x)$, that is, $F(x) = 0$. Solution at $t = 6$; (b) linear potential field $V(x) = -2x$, that is, $F(x) = 2$. Solution at $t = 4$.

We start with the case of a free Brownian particle, that is, for $V(x)$ constant, which implies $F(x) = 0$. In figure 4(a) we show a plot of $f(x, p, t)$, at the instant of time $t = 6$, and also the corresponding contour lines, since these two quantities together provide a good picture of how the dynamics of the Brownian particle evolves. The effect of absorbing BCs may be more clearly seen from the contour lines. For this case we also observe that (44) is verified.

The case of the linear potential $V(x) = -2x$ i.e. $F(x) = 2$ is presented in figure 4(b), for the instant $t = 4$. The $f(x, p, t)$ profile and the contour lines are now asymmetric (shifted to the right boundary) and the particle is not going to return to the domain. The escape from the domain is due to absorbing BCs. As one would expect, although we do not plot it here, for $V(x) = 2x$ that is for $F(x) = -2$, $f(x, p, t)$ and the contour lines will be shifted to the left boundary. For the linear potential, the equality (44) does not hold.

We briefly mention the case of a harmonic potential $V(x) = x^2/2$ that is for $F(x) = -x$. This is a symmetric (about $x = 0$) and attractive (confining) potential. We do not show any figure for this case because the numerical solution vanishes before it reaches the boundaries. The particle is confined in the central part of the domain. A contrasting case is a harmonic potential $V(x) = -x^2/2$ for which $F(x) = x$. This is a symmetric repulsive (de-confining) potential. The results for this potential are shown in figure 5(a), for $t = 5$. We now expect the particle to be symmetrically pushed away from the interior of the domain both to the left and to the right. A combined effect of this potential and absorbing BCs is that the particle will be symmetrically absorbed in both boundaries and (44) is satisfied.

The Kramers equation for a periodic potential has been considered in the literature (see, for example [8, 9]). We have solved the Kramers equation for three periodic potentials and for finite geometries.

We first deal with two periodic potentials for which figures are plotted for $t = 6$. We show $f(x, p, t)$ and the contour lines for $V(x) = \sin(\pi x/10)$ that is for $F(x) = -(\pi/10)\cos(\pi x/10)$ in figure 5(b). In this case the force remains negative throughout

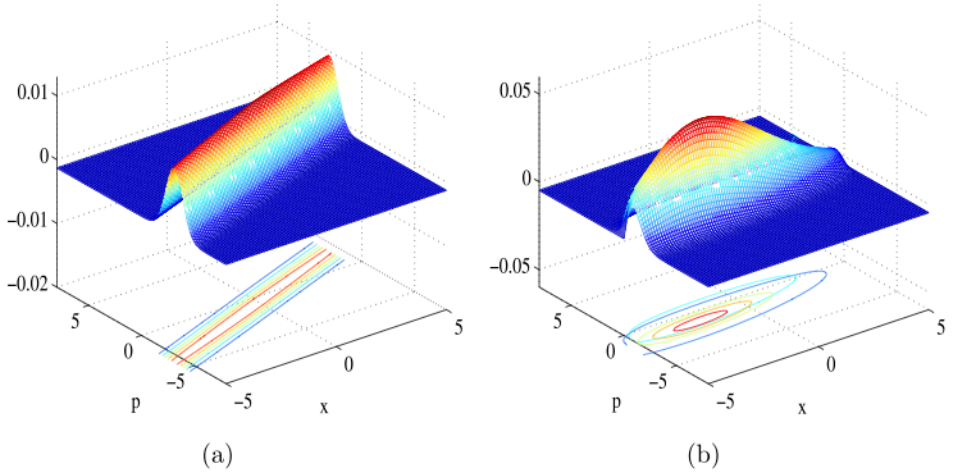

Figure 5. Surfaces and contour lines of the numerical solution $f(x, p, t)$ with absorbing boundary conditions (43); (a) harmonic potential field $V(x) = -x^2/2$, that is, $F(x) = x$. Solution at $t = 5$; (b) periodic potential field $V(x) = \sin(\pi x/10)$, that is, $F(x) = -(\pi/10)\cos(\pi x/10)$. Solution at $t = 6$.

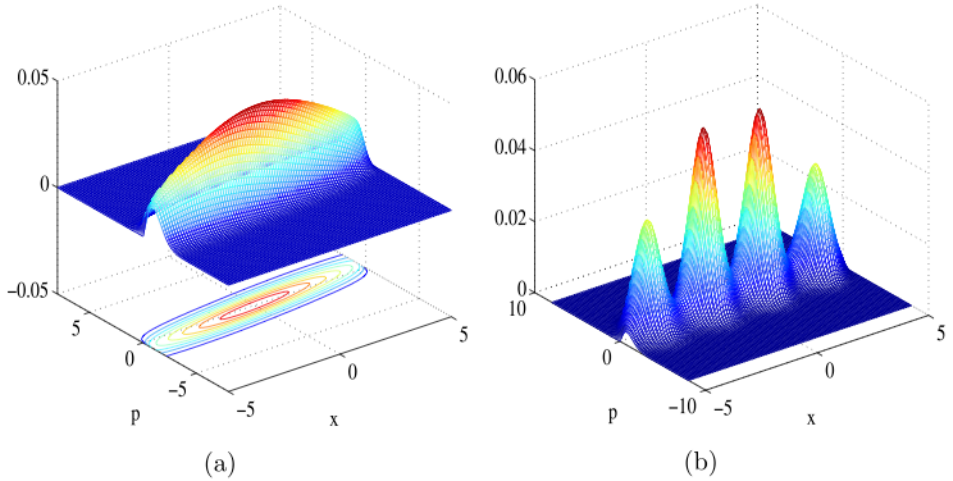

Figure 6. Surfaces and contour lines of the numerical solution of $f(x, p, t)$ with absorbing boundary conditions (43); (a) periodic potential field $V(x) = \cos(\pi x/10)$, that is, $F(x) = (\pi/10)\sin(\pi x/10)$. Solution at $t = 6$; (b) periodic potential field $V(x) = \cos(8\pi x/10)$, that is, $F(x) = (8\pi/10)\sin(8\pi x/10)$. Solution at $t = 30$.

the spatial domain $-5 \leqslant x \leqslant 5$ as in the case of $F(x) = -2$ mentioned earlier; $f(x, p, t)$ for this case shows a leftward shift. The particle now escapes asymmetrically from the domain. For the second periodic potential, shown in figure 6(a), $V(x) = \cos(\pi x/10)$ that is for $F(x) = (\pi/10)\sin(\pi x/10)$, we note that $V(x)$ is symmetric in x and, as in the cases of symmetric potentials considered in within this section, $f(x, p, t)$ is expected to undergo a

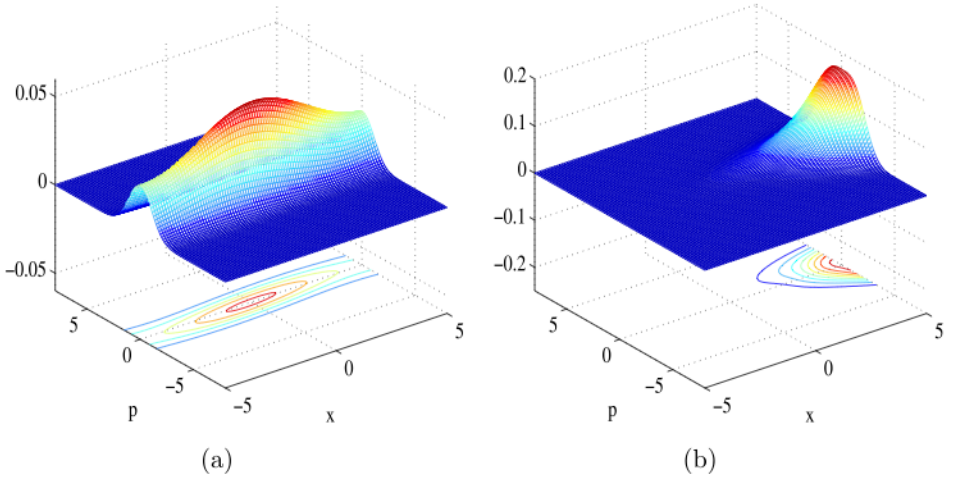

Figure 7. Surfaces and contour lines of the numerical solution $f(x, p, t)$ with reflecting boundary conditions (45). (a) Homogeneous potential field, that is, $F(x) = 0$. Solution at $t = 6$; (b) potential field $V(x) = -2x$, that is, $F(x) = 2$. Solution at $t = 4$.

symmetric evolution. In this case the particle escapes symmetrically from the domain and satisfies (44).

The third periodic potential is shown in figure 6(b), where $V(x) = \cos(8\pi x/10)$ i.e. $F(x) = (8\pi/10)\sin(8\pi x/10)$. This potential is chosen to have a shorter period, and the time $t = 30$ provides a longtime profile of $f(x, p, t)$.

In the next section we do a similar study, now assuming reflecting BCs.

4.2. Reflecting BCs

Unlike the absorbing BCs discussed in the previous section, the reflecting BCs do not allow the Brownian particle to escape from the domain and the particle is now confined within the domain. We have looked at these BCs in section 2, from the perspective of particle flux conservation. The reflecting BCs for our domain are specified by

$$f(-5, p, t) = f(-5, -p, t) \qquad \text{and} \qquad f(5, p, t) = f(5, -p, t) \quad \text{for all } p. \tag{45}$$

We have studied these BCs for the same potential fields as in the case of two absorbing BCs. From numerical solutions we have found that for symmetric (even in x) potentials and hence for antisymmetric (odd in x) forces, there are additional symmetry relations

$$f(-5, p, t) = f(5, p, t) \qquad \text{for all } p. \tag{46}$$

Like (44), the relation (46) is empirical and is established through a study of numerical solutions. In the cases for which (46) is valid, $f(x, p, t)$ behaves as if it has a periodicity in x seen from one end of the domain to the other with end points satisfying (46). This additional symmetry of $f(x, p, t)$ results from a combination of the reflecting BCs given by (45) and the type of potential field. For the other cases in which the potentials are odd in x and hence the forces are even in x, the numerical solutions show that the Brownian particle is asymmetrically confined within the domain with the peaking of $f(x, p, t)$ at one boundary. These cases are illustrated in figures 7(b) and 8(b), for the forces $F(x) = 2$ and $F(x) = -(\pi/10)\cos(\pi x/10)$ respectively.

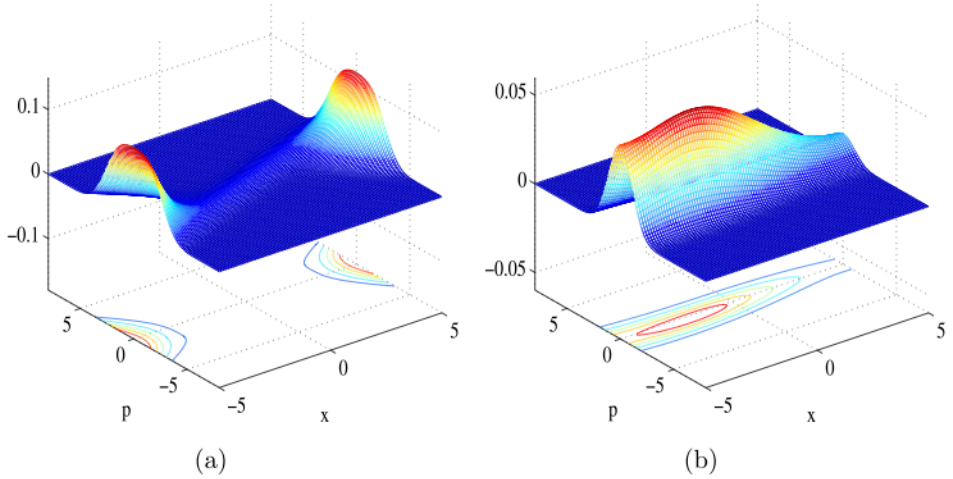

Figure 8. Surfaces and contour lines of the numerical solution $f(x, p, t)$ with reflecting boundary conditions (45). (a) Potential field $V(x) = -x^2/2$, that is, $F(x) = x$. Solution at $t = 5$; (b) potential field $V(x) = \sin(\pi x/10)$, that is, $F(x) = -(\pi/10)\cos(\pi x/10)$. Solution at $t = 6$.

The free Brownian particle case i.e. $F(x) = 0$ is illustrated in figure 7(a) for $t = 6$. In this case condition (46) is verified.

The case $V(x) = -2x$, that is, for $F(x) = 2$ is shown in Figure 7(b), for $t = 4$, where we see that $f(x, p, t)$ peaks at the right boundary. From this figure it is easy to predict that for $V(x) = 2x$ i.e. for $F(x) = -2$, $f(x, p, t)$ will peak at the left boundary.

The numerical solution $f(x, p, t)$ and its contour lines for $V(x) = -x^2/2$ i.e. $F(x) = x$ is shown in figure 8(a) for $t = 5$, and we observe condition (46) is satisfied.

We now present the same periodic potential cases as in the previous sub-section, for the instant of time $t = 6$. Figure 8(b) is shown for the case $V(x) = \sin(\pi x/10)$ which is odd in x and hence $F(x) = -(\pi/10)\cos(\pi x/10)$ is even in x. Note that in this case the force remains negative throughout the domain. It thus acts like a directed force similar to $F(x) = -2$ mentioned earlier, and $f(x, p, t)$ peaks predominantly at the left boundary. The situation is reverse for $V(x) = \cos(\pi x/10)$ i.e. $F(x) = (\pi/10)\sin(\pi x/10)$. Now the force, like $F(x) = x$, changes sign with respect to $x = 0$ and does not act like a directed force throughout the domain. As in the case of $F(x) = x$, a combination of the reflecting BCs and the type of force leads to the relation (46). This situation is illustrated in figure 9(a).

As with absorbing BCs, we consider the third periodic potential given by $V(x) = \cos(8\pi x/10)$ that is $F(x) = (8\pi/10)\sin(8\pi x/10)$, shown in figure 9(b) for a long time profile of $f(x, p, t)$, that is, $t = 30$. The contour lines for $f(x, p, t)$ for the third periodic potential are not shown because the profiles of $f(x, p, t)$ for absorbing and reflecting BCs well illustrate the longtime behaviour. If we compare figure 9(b) with the absorbing case, plotted in figure 6(b), we can see the figures are different and the two peaks near the left and right boundaries are lower for the absorbing case.

In concluding this section, we briefly consider a scenario of mixed BCs, namely one (left) reflecting BC and one (right) absorbing BC. For our domain we have the conditions

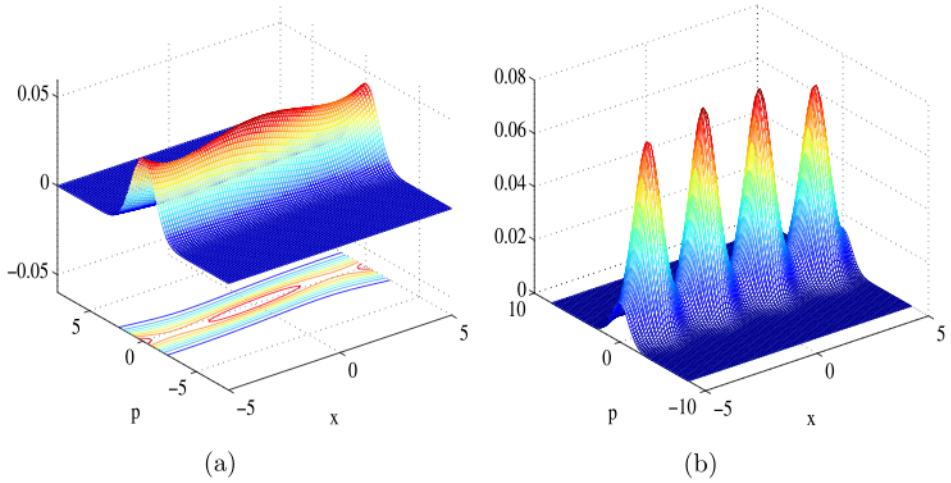

Figure 9. Surfaces and contour lines of the numerical solution $f(x, p, t)$ with reflecting boundary conditions (45). (a) Potential field $V(x) = \cos(\pi x/10)$, that is, $F(x) = (\pi/10)\sin(\pi x/10)$. Solution at $t = 6$; (b) potential field $V(x) = \cos(8\pi x/10)$, that is, $F(x) = (8\pi/10)\sin(8\pi x/10)$. Solution at $t = 30$.

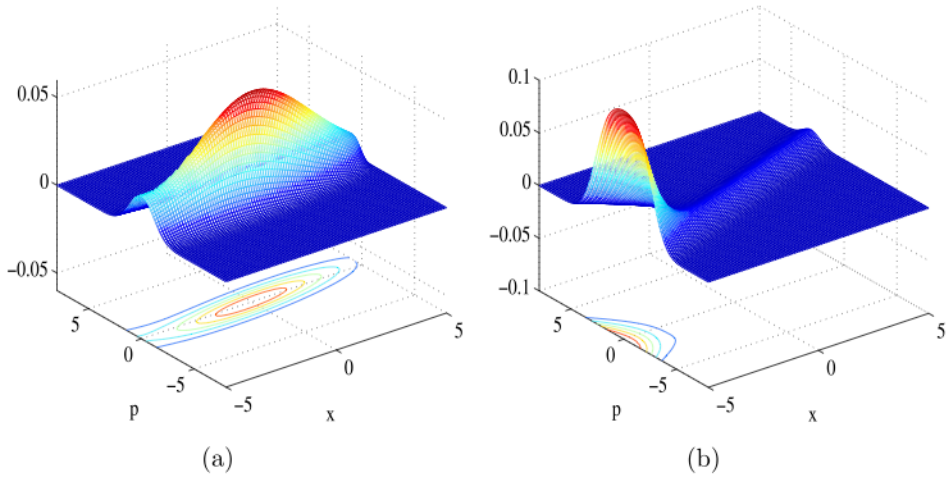

Figure 10. Surfaces and contour lines of the numerical solution $f(x, p, t)$ with left reflecting boundary conditions and right absorbing boundary conditions (47). (a) Homogeneous potential field, that is, $F(x) = 0$. Solution at $t = 5$; (b) potential field $V(x) = -x^2/2$, that is, $F(x) = x$. Solution at $t = 5$.

$$f(-5, p, t) = f(-5, -p, t), \qquad f(5, p, t) = 0, \quad \text{for } p < 0. \tag{47}$$

This scenario is of physical relevance e.g. in connection with studies of first passage times [33]; for a recent review, see [3]. In order to illustrate the behaviour of solutions for BCs (47) we have considered only two potential fields: $V(x)$ constant i.e. $F(x) = 0$, and $V(x) = -x^2/2$

i.e. $F(x) = x$. The results for $f(x, p, t)$ and contour lines are shown in figure 10 for both cases at $t = 5$. Figure 10(a) can be compared with figures 4(a) and 7(a); figure 10(b) can be compared with figures 5(a) and 8(a). This comparison shows how a combination of one reflecting BC and one absorbing BC affects the spatio-temporal dynamics of the Brownian particle. We note that for one or both absorbing BCs, the probability distribution $f(x, p, t)$ will decay in time. Hence for these cases the survival probability of the Brownian particle is of theoretical and practical interest. This leads us to the next section.

4.3. Spatial density $n(x, t)$ and survival probability $N(t)$

In this section we use numerical solutions for $f(x, p, t)$ to calculate two quantities which complement our studies of the Kramers equation for finite geometries. These two quantities are defined as

$$n(x, t) = \int_{-\infty}^{\infty} f(x, p, t)\mathrm{d}p \tag{48}$$

and

$$N(t) = \int_{x_L}^{x_R} n(x, t)\mathrm{d}x. \tag{49}$$

The function $N(t)$ which we refer to as global density becomes the survival probability in the case of one or both absorbing BCs. The number density $n(x, t)$ illustrates an unusual feature of the Kramers equation with absorbing BCs. This feature is more clearly seen at the level of $n(x, t)$ than with $f(x, p, t)$ itself. In order to see this let us recall the Fickian diffusion equation (without a potential field, for simplicity)

$$\frac{\partial n_F}{\partial t}(x, t) = D\frac{\partial^2 n_F}{\partial x^2}(x, t); \qquad x = [x_L, x_R], \ t > 0,$$

for two absorbing BCs at $x = x_L$ and at $x = x_R$. These two BCs are usually assumed to be (on physical ground)

$$n_F(x_L, t) = 0; \qquad n_F(x_R, t) = 0, \qquad t > 0. \tag{50}$$

For this case we are denoting the density by $n_F(x, t)$ (F for Fickian). Next let us calculate $n(x, t)$ and $N(t)$ from our numerical solutions of the Kramers equation, according to (48) and (49) respectively. As expected, the value of $N(t)$ will decrease in the case of absorbing BCs whereas for the reflecting BCs it is still the same. We may expect that $n(x, t)$, which at long times tend to $n_F(x, t)$, will also vanish at the absorbing boundaries as in (50). In fact $n(x, t)$ does not vanish exactly at $x = x_L$ and $x = x_R$. This feature of $n(x, t)$ is illustrated for the following cases: figure 11(a) for $F(x) = 0$, figure 12(a) for $F(x) = 2$, figure 13(a) for $F(x) = x$, figure 14(a) for $F(x) = (\pi/10)\sin(\pi x/10)$ and figure 15(a) for $F(x) = -(\pi/10)\cos(\pi x/10)$. Note that $n(x, t)$ in these figures refers to the number density obtained through the Kramers equation and (48).

The difference between $n_F(x, t)$ and $n(x, t)$ at the absorbing boundaries can be understood in this way. On physical ground we expect that $n_F(x, t)$ vanishes at the absorbing boundaries. However if we recall the absorbing BCs on $f(x, p, t)$ at the same boundaries, we note that $f(x, p, t)$ is assumed to vanish for only one half range of p's at each boundary. The other half range of p's makes a non-zero contribution to $n(x, t)$ after the integration over p's according to (48). Hence $n(x, t)$ remains non-zero at absorbing boundaries even at long times. This feature has been discussed in the literature and we refer to [6, 7] as an example.In [6, 7] a semi-infinite geometry is considered and the analysis is based on only stationary

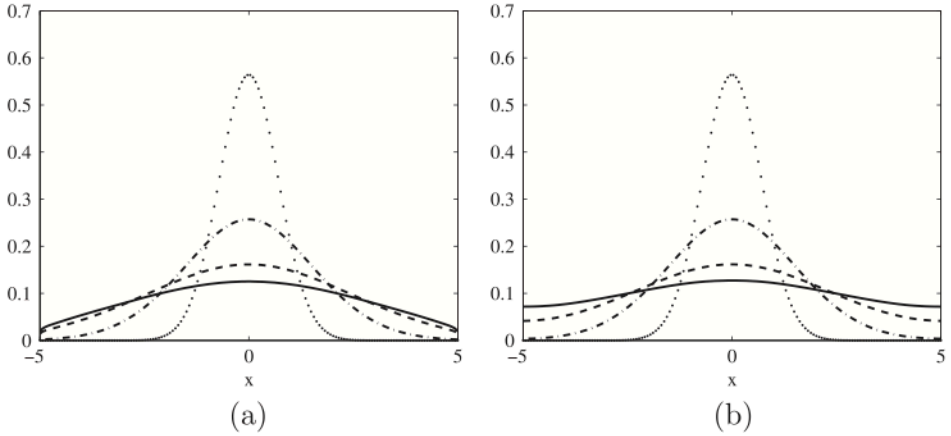

Figure 11. Plots of $n(x, t)$ for $t = 0(\cdots)$, $t = 2(- \cdot -)$, $t = 4(- -)$, $t = 6(-)$ for $F(x) = 0$ with: (a) absorbing boundary conditions (43). The values of $N(t)$ are respectively $N(0) = 1$, $N(2) = 0.9980$, $N(4) = 0.9508$, $N(6) = 0.8634$; (b) reflecting boundary conditions (45). The values of $N(t)$ are respectively $N(0) = 1$, $N(2) = 0.9998$, $N(4) = 0.9973$, $N(6) = 0.9952$.

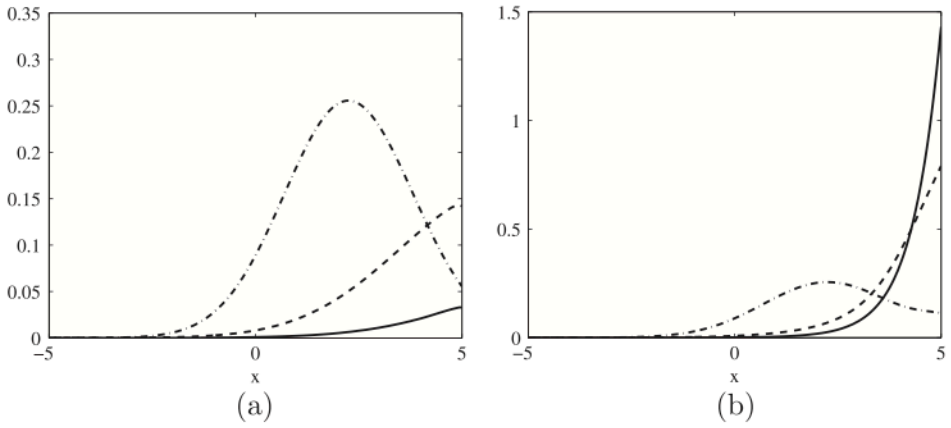

Figure 12. Plots of $n(x, t)$ for $t = 2(- \cdot -)$, $t = 4(- -)$, $t = 6(-)$ for $F(x) = 2$ with: (a) absorbing boundary conditions (43). The values of $N(t)$ are respectively $N(0) = 1$, $N(2) = 0.9589$, $N(4) = 0.3383$, $N(6) = 0.05687$; (b) reflecting boundary conditions (45). The values of $N(t)$ are respectively $N(0) = 1$, $N(2) = 0.9989$, $N(4) = 0.9921$, $N(6) = 0.9857$.

solution of the Kramers equation without a potential field. If we consider our numerical results at long time for the density profile near the absorbing boundary at $x = 0$, then our results and theirs are consistent with each other. Both indicate that the density profile $n(x, t)$, for long times, does not vanish at $x = 0$; it vanishes a little away from $x = 0$. We observe from figures 12(a) to 15(a) that $n(x, t)$ can be noticeably different from zero at the absorbing boundaries, due to potential fields.

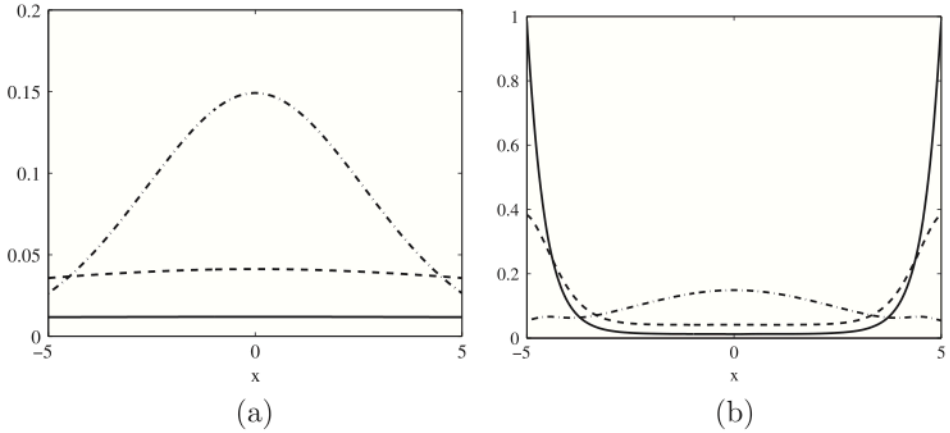

Figure 13. Plots of $n(x, t)$ for $t = 2(- \cdot -)$, $t = 4(- -)$, $t = 6(-)$ for $F(x) = x$ with: (a) absorbing boundary conditions (43). The values of $N(t)$ are respectively $N(0) = 1$, $N(2) = 0.9352$, $N(4) = 0.3930$, $N(6) = 0.1189$; (b) reflecting boundary conditions (45). The values of $N(t)$ are respectively $N(0) = 1$, $N(2) = 0.9989$, $N(4) = 0.9923$, $N(6) = 0.9803$.

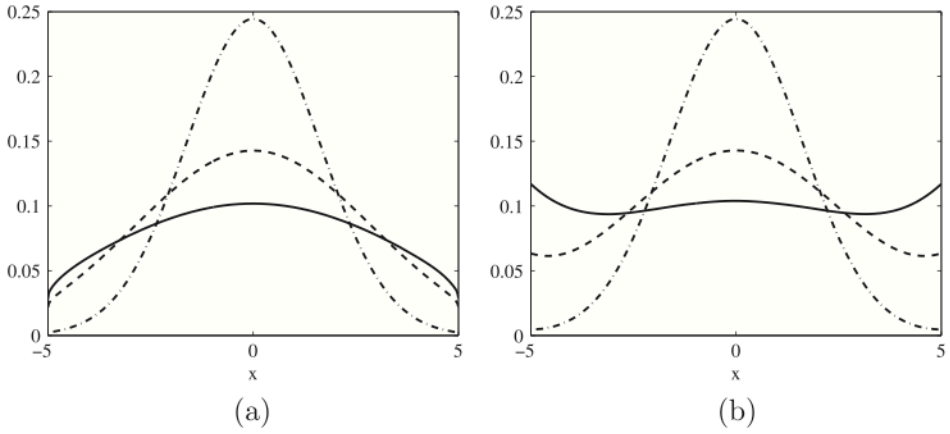

Figure 14. Plots of $n(x, t)$ for $t = 2(- \cdot -)$, $t = 4(- -)$, $t = 6(-)$ for $F(x) = (\pi/10)\sin(\pi x/10)$ with: (a) absorbing boundary conditions (43). The values of $N(t)$ are respectively $N(0) = 1$, $N(2) = 0.9977$, $N(4) = 0.9280$, $N(6) = 0.7969$; (b) reflecting boundary conditions (45). The values of $N(t)$ are respectively $N(0) = 1$, $N(2) = 0.9999$, $N(4) = 0.9987$, $N(6) = 0.9977$.

For the reflecting BCs, $n(x, t)$ can be significantly affected by non-zero potential fields, as can be seen in figures 13(b)–15(b). The asymmetry in $n(x, t)$, as shown in figures 15(a) and (b), is a consequence of the asymmetry in $f(x, p, t)$ in these cases; $n(x, t)$ is shifted toward the left boundaries (discussed in section 4.2). While $n(x, t)$ is a local number density, $N(t)$ given by (49) can be viewed as a global density. For each of the Figures 11–13, the values of $N(t)$ are cited (see figure legends) for three values of time. For both absorbing BCs,

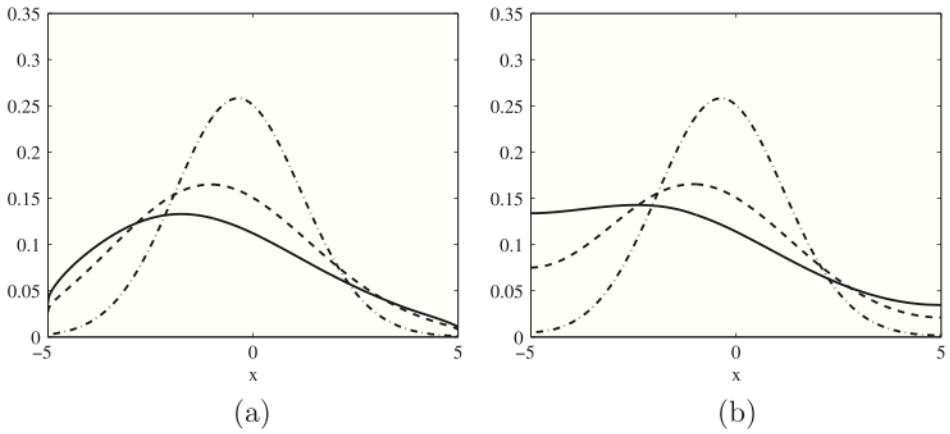

Figure 15. Plots of $n(x, t)$ for $t = 2(- \cdot -)$, $t = 4(- -)$, $t = 6(-)$ for $F(x) = -(\pi/10)\cos(\pi x/10)$ with: (a) absorbing boundary conditions (43). The values of $N(t)$ are respectively $N(0) = 1$, $N(2) = 0.9983$, $N(4) = 0.9462$, $N(6) = 0.8459$; (b) reflecting boundary conditions (45). The values of $N(t)$ are respectively $N(0) = 1$, $N(2) = 0.9999$, $N(4) = 0.9990$, $N(6) = 0.9983$.

$N(t)$ decreases in time. But for both reflecting BCs, $N(t)$—within numerical accuracy—remains constant in time because the Brownian particle is now confined within the domain.

5. Conclusion and outlook

In this paper we have presented a detailed numerical study of the time-dependent Kramers equation without and with potential fields, for finite geometries and in one spatial dimension. The effect of finite geometries is included through absorbing and reflecting BCs due to Wang and Uhlenbeck [41]. The emphasis in our study is a numerical solution of the Kramers equation. The Brownian particle is assumed to be initially located at $(x, p) = (0, 0)$. We have considered a finite domain $x_L \leqslant x \leqslant x_R$ with $x_L = -x_R$ and a momentum space domain as $-\infty < p < \infty$. To obtain numerical solutions at each time we have used an explicit numerical method whose properties of convergence such as its stability conditions have been discussed in detail. These properties allow us to successfully obtain accurate numerical solutions. For the choice of the domain ($x_R = -x_L$) the initial position of the particle is symmetrical with respect to both boundaries. And we take the initial distribution to be symmetrical also in p-space. If we envisage an initial distribution not centred at $(x, p) = (0, 0)$ such as one with a shift (small compared to the length of half the domain) to the right or left of $x = 0$ in x-space and with a shift up or down in p-space, then we still expect the general findings in section 4 to hold although the additional symmetries given, respectively, by (44) for absorbing BCs and by (46) for reflecting BCs, may not hold. We may add that the additional symmetry relations arise when both boundaries are of the same type.

One highlight of our work is to consider a few potentials $V(x)$ some of which are symmetrical about $x = 0$ while others are not, and to numerically study an interplay between the BCs (both absorbing and reflecting) and the type of potentials to see how this interplay determines profiles for $f(x, p, t)$ and contour lines. This has also led us to find some additional symmetry relations for $f(x, p, t)$ in the case of potentials of certain symmetry. The

potentials we have considered are of theoretical interest and experimental relevance. For an absorbing BC there is a conceptual element of interest regarding the vanishing of Brownian particle density $n(x, t)$ at the boundary itself or a little away from it. We have illustrated this feature with a few examples of potentials. Among physical quantities and scenarios which can be studied with the type of numerical solutions reported in this paper, some are briefly mentioned below. With one or both absorbing BCs and without and with potential fields, one can consider first passage problems (see [3] for a recent review). A quantity of considerable interest is mean-square displacement $<x^2(t)>$ for underdamped Brownian motion in finite geometries. A bistable potential, symmetrical and asymmetrical, with a reflecting BC, say at the left and an absorbing BC at the right is a topic by itself and leads to escape from a well, etc. We also mention partially absorbing and partially reflecting BCs. A time-dependent external field in addition to a potential $V(x)$, and a consideration of more than one spatial dimension will extend the work beyond what has been reported here.

Recently several research papers have been appearing on the generalized Kramers equation. This equation consists of considering a factional derivative in time [28–30]. It would be of interest to see if and how the type of findings we report in this paper would be affected in the case of a generalized Kramers equation. However, this problem requires a separate study. A generalization of the numerical method presented here can be done, by noticing that in the direction x and p the discretizations can be the same as also the treatment of the BCs. The main change is how the iteration in time is implemented. The theoretical convergence analysis of such numerical method is more demanding and may require a different approach.

Acknowledgments

Research supported by CMUC and FCT (Portugal) through European program COMPETE under the project PEst-C/MAT/UI0324/2013.

References

[1] Araújo A, Das A K, Neves C and Sousa E 2013 Numerical solution for a non-Fickian diffusion in a periodic potential *Commun. Comput. Phys.* **13** 502–25
[2] Bicout D J, Berezhkovskii A M, Szabo A and Weiss G H 1999 Kramers-like turnover activationless rate processes *Phys. Rev. Lett.* **83** 1279–82
[3] Bray A J, Majumdar S N and Schehr G 2013 Persistence and first passage properties in nonequilibrium systems *Adv. Phys.* **62** 225–361
[4] Brinkman H C 1956 Brownian motion in a field of force and the diffusion theory of chemical reactions *Physica* **22** 29–34
[5] Boutet de Monvel A and Dita P 1990 Analytic solution for a boundary value problem in the theory of Brownian motion *J. Phys. A: Math. Gen.* **23** 895–8
[6] Burscha M A and Titulaer U M 1981 The kinetic boundary layer for the Fokker–Planck equation: Selectively absorbing boundaries *J. Stat. Phys.* **26** 59–71
[7] Burscha M A and Titulaer U M 1981 The kinetic boundary layer for the Fokker–Planck equation with absorbing boundary *J. Stat. Phys.* **25** 569–82
[8] Caratti G, Ferrando R, Spadacini R and Tommei G E 1996 Noise-activated diffusion in the egg-carton potential *Phys. Rev.* E **54** 4708
[9] Caratti G, Ferrando R, Spadacini R and Tommei G E 1998 The Kramers problem in 2D-coupled periodic potentials *Chem. Phys.* **235** 157–70
[10] Cartling B 1987 Kinetics of activated processes from nonstationary solutions of the Fokker–Planck equation for a bistable potential *J. Chem. Phys.* **87** 2638–48

[11] Cartling B 1989 Brownian motion model of activated transitions in a periodic potential *J. Chem. Phys.* **90** 1819–31
[12] Coffey W T, Crothers D S and Titov S V 2001 Escape times for rigid Brownian rotators in a bistable potential from the time evolution of the Green function and the characteristic time of the probability evolution *Physica* A **298** 330350
[13] Coffey W T, Kalmykov Y U and Titov S V 2001 Inertial effects in the nonlinear transient relaxation of Brownian particles in strong external electric fields *J. Chem. Phys.* **115** 9895
[14] Coffey W T, Kalmykov Y U and Titov S V 2012 *The Langevin Equation* 3rd edn (Singapore: World Scientific)
[15] Crank J 1956 *The Mathematics of Diffusion* (Oxford: Oxford University Press)
[16] Crothers D S F 2007 *Semiclassical Dynamics and Relaxation* (Berlin: Springer)
[17] Das A K 1991 A non-Fickian diffusion equation *J. Appl. Phys.* **70** 1355–8
[18] Davis P J 1979 *Circulant Matrices* (New York: Wiley-Interscience)
[19] Duck P W, Marshall T W and Watson E J 1986 First-passage times for the Uhlenbeck–Ornstein process *J. Phys. A: Math. Gen.* **19** 3545–58
[20] Fok J C M, Guo B and Tang T 2002 Combined Hermite spectral-finite difference method for the Fokker–Planck equation *Math. Comput.* **71** 1497–528
[21] Guo B-Y and Wang T J 2009 composite generalized Laguerre-Legendre spectral method with domain decomposition and its application to Fokker–Planck equation in an infinite channel *Math. Comput.* **78** 129–51
[22] Gustafsson B, Kreiss H-O and Oliger J 1995 *Time Dependent Problems and Difference Methods* (New York: Wiley-Interscience)
[23] Hindmarsh A C, Gresho P M and Griffiths D F 1984 The stability of explicit Euler time-integration for certain finite difference approximations of the multi-dimensional advection-diffusion equation *Int. J. Numer. Methods Fluids* **4** 853–97
[24] Kalmykov Y P, Coffey W T and Titov S V 2006 Thermally activated escape rate for a Brownian particle in a double-well potential for all values of the dissipation *J. Chem. Phys.* **124** 024107
[25] Lax P D 1961 On the stability of difference approximations to solutions of hyperbolic equations with variable coefficients *Commun. Pure Appl. Math.* **14** 497
[26] Lax P D 1966 On stability of difference schemes: a sharp form of Garding inequality *Commun. Pure Appl. Math.* **19** 473
[27] Marshall T W and Watson E J 1985 A drop of ink falls from my pen łdots It comes to earth, I know not when *J. Phys. A: Math. Gen.* **18** 3531–59
[28] Metzler R 2000 Generalized Chapman–Kolmogorov equation: a unifying approach to the description of anomalous transport in external fields *Phys. Rev.* E **62** 6233–45
[29] Metzler R and Klafter J 2000 Subdiffusive transport close to thermal equilibrium: from the Langevin equation to fractional diffusion *Phys. Rev.* E **61** 6308–11
[30] Metzler R and Klafter J 2004 The restaurant at the end of the random walk: recent developments in the description of anomalous transport by fractional dynamics *J. Phys. A: Math. Gen.* **37** 161–208
[31] Moore P and Flaherty J 1992 Adaptive local overlapping grid methods for parabolic systems in two space dimensions *J. Comput. Phys.* **98** 5463
[32] Morton K W 1996 *Numerical Solution of Convection Diffusion Problems* (London: Chapman and Hall)
[33] Redner S 2001 *A Guide to First-Passage Processes* (Cambridge: Cambridge University Press)
[34] Richtmyer R D and Morton K W 1967 *Difference Methods for Initial Value Problems* (New York: Wiley-Interscience)
[35] Risken H 1989 *The Fokker–Planck Equation* (Berlin: Springer)
[36] Singer A and Schuss Z 2005 Asymptotic solution of Wang–Uhlenbeck recurrence time problem *Phys. Rev. Lett.* **95** 110601
[37] Sod G A 1988 *Numerical Methods in Fluid Dynamics: Initial and Initial Boundary-Value Problems* (Cambridge: Cambridge University Press)
[38] Sousa E 2009 On the edge of stability analysis *Appl. Numer. Math.* **59** 1322 –1336
[39] Stratonovich R L 1963 *Topics in the Theory of Random Noise* vol 1 (London: Gordon and Breach)
[40] Shen J 2000 Stable and efficient spectral methods in unbounded domains using Laguerre functions *SIAM J. Numer. Anal.* **38** 1113–33
[41] Wang M C and Uhlenbeck G E 1945 On the theory of the Brownian motion II *Rev. Mod. Phys.* **17** 323–43

[42] Wang T-J and Guo B-Y 2008 Composite generalized Laguerre–Legendre pseudospectral method for Fokker–Planck equation in an infinite channel *Appl. Numer. Math.* **58** 1448–66
[43] Tang T 1993 The Hermite spectral method for Guassian type functions *SIAM J. Sci. Comput.* **14** 594–606
[44] Zorzano M P, Mais H and Vasquez L 1999 Numerical solution of two dimensional Fokker–Planck equations *Appl. Math. Comput.* **98** 109–17